International Journal of Innovative Computing, Information and Control
Volume **8**, Number **4**, April **2012**

 ISSN 1349-4198
pp. **2901–2914**

DESIGN OF A DUAL-INPUT BUCK-BOOST CONVERTER FOR MOBILE BACK-LIGHTING APPLICATIONS

Kei Eguchi[1], Sawai Pongswatd[2], Amphawan Julsereewong[2]
Ichirou Oota[3], Shinya Terada[3] and Hirofumi Sasaki[4]

[1]Department of Information Electronics
Fukuoka Institute of Technology
3-30-1 Wajiro-Higashi, Higashi-Ku, Fukuoka 811-0295, Japan
eguchi@inass.org

[2]Faculty of Engineering
King Mongkut's Institute of Technology Ladkrabang
Ladkrabang, Bangkok 10520, Thailand
{ klsawai; kcamphaw }@kmitl.ac.th

[3]Department of Information and Communication
Kumamoto National College of Technology
2659-2, Suya, Koushi, Kumamoto 861-1102, Japan
oota-i@tc.knct.ac.jp; terada@ee.knct.ac.jp

[4]Tokai University
9-1-1 Toroku, Kumamoto-shi, Kumamoto 862-8652, Japan
hsasaki@ktmail.tokai-u.jp

Received February 2011; revised July 2011

Abstract. *For mobile back-lighting applications, a dual-input white LED (WLED) driver using a bi-direction buck-boost converter is proposed in this paper. The proposed driver has two input terminals: battery input V_{in1} and solar-cell input V_{in2}. Unlike conventional drivers using boost converters, step-up SC DC-DC converters, and so on, the proposed converter drives the anode and the cathode of LEDs by using the solar-cell's voltage and the negative stepped-down voltage, respectively. Furthermore, by converting solar energy, the proposed driver can charge a rechargeable battery when the LED backlight is standby mode. Therefore, the proposed driver can achieve long battery lifetime. The validity of the proposed driver is confirmed by SPICE simulations and experiments. SPICE simulations show that the proposed driver can offer the sufficient voltage to drive LEDs by using solar energy and battery energy in spite of the variation in V_{in2}. Furthermore, by employing a bi-direction buck-boost converter, the proposed driver provides us to realize long battery lifetime, because the battery charge process was confirmed by experiments.*

Keywords: Switching converters, Buck-boost converters, White LEDs, Individual mode switching, Clean energy, Solar cells

1. **Introduction.** A switching converter has been used as a driver circuit for the white LED (WLED) of small color displays in portable devices. By converting the battery voltage which is 3 $\sim$ 4.2 V (Typ. = 3.7 V), the switching converter provides 3.5 $\sim$ 3.8 V to drive WLEDs at up to 20 mA. In previous studies, several types of WLED drivers have been proposed: the inductor-based driver using a boost converter [1-6], the switched-capacitor (SC)-based driver using a step-up SC DC-DC converter [7-26], the $-0.5\times$ charge-pump driver [27], and so on.

In the boost converter [1-6] and the SC DC-DC converters [7-26], the positive stepped-up voltage is generated to drive LED's anodes. The features of the step-up SC DC-DC converter are thin circuit composition, light-weight, no flux of magnetic induction, and so on. On the other hand, the features of the inductor-based converter such as a boost converter are simple structure and high efficiency. Furthermore, the inductor-based converter can achieve high power efficiency, because the output voltage can be adjusted by controlling the duty factor of clock pulses. However, when LEDs are mismatched, WLED drivers using these step-up converters must switch to step-up mode due to the bad forward voltage of only one LED.

To overcome this weak point, the $-0.5\times$ charge-pump driver has been proposed [27]. The converter realizing negative-conversion drives only the highest LED with the bad forward voltage through the $-0.5\times$ negative path, while the LEDs with lower forward voltages remain in the $1\times$ mode. Therefore, the negative charge-pump can achieve high power efficiency. This technique is called the individual mode switching. Furthermore, the charge-pump has the same feature as SC DC-DC converters, because the charge-pump is a family of SC DC-DC converters. However, it is difficult to improve power efficiency further in the $-0.5\times$ mode, because the conversion ratio of charge-pumps is predetermined by circuit structure. In the $-0.5\times$ charge-pump, the energy loss caused by output regulation becomes large when output voltage V_{out} is $V_{out} \gg 3.5 \sim 3.8$ V.

To solve this problem, a dual-input WLED driver using a bi-direction buck-boost converter is proposed in this paper. The proposed driver has two input terminals: battery input V_{in1} and solar-cell input V_{in2}. By using individual mode switching, the proposed converter drives the LED's anode when the voltage of solar-cells is sufficient to turn on LEDs. On the other hand, when the voltage of solar-cells is insufficient, the proposed converter drives the anode and the cathode of LEDs by using the solar-cell's voltage and the negative stepped-down voltage, respectively. Unlike the negative charge-pump, the output voltage of the proposed driver can be adjusted by controlling the duty factor of clock pulses, because the proposed driver is an inductor-based converter. Furthermore, by converting solar energy, the proposed driver can charge a rechargeable battery when the LED back-light is standby mode. Therefore, unlike conventional drivers using boost converters [1-6], step-up SC DC-DC converters [7-26], and so on, the proposed driver can achieve long battery lifetime. To confirm the validity of circuit design, SPICE simulations and experiments are performed concerning the proposed driver.

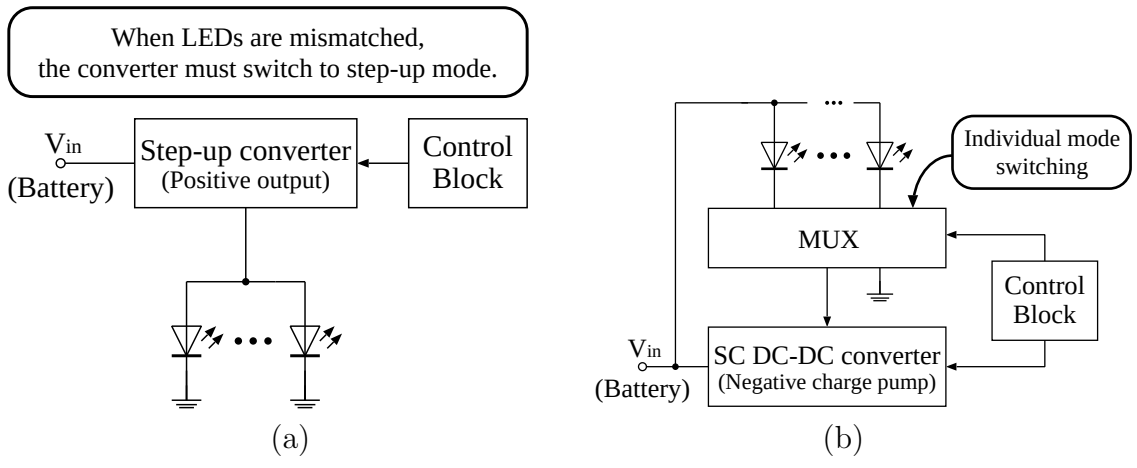

FIGURE 1. Block diagram of conventional drivers, (a) WLED driver using a step-up converter, (b) Negative switched-capacitor-based driver

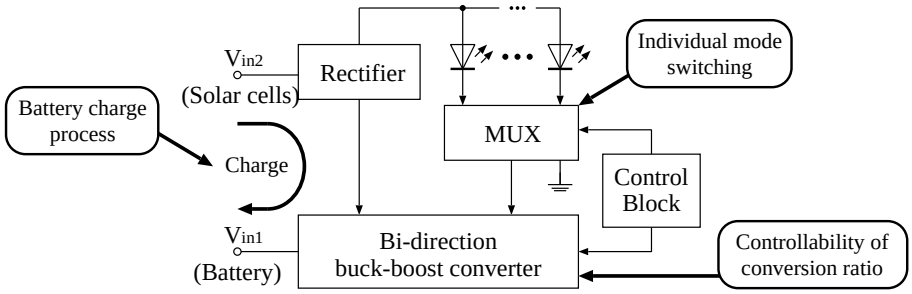

FIGURE 2. Block diagram of the proposed driver using a bi-direction buck-boost converter

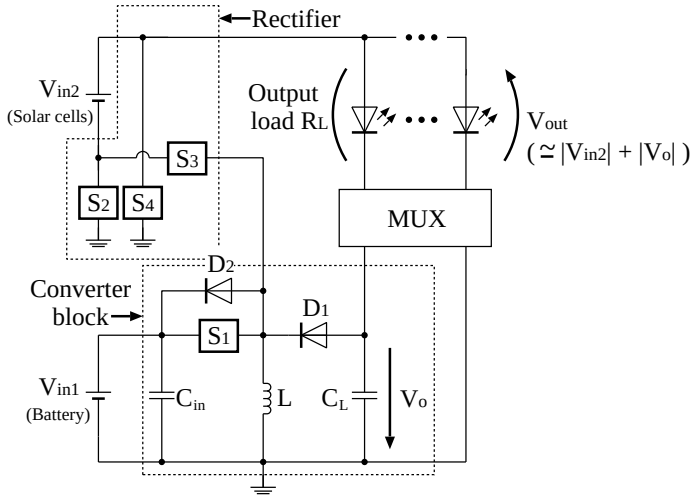

FIGURE 3. Proposed driver using a bi-direction buck-boost converter

2. **Conventional WLED Driver.** Figure 1 shows the block diagram of the conventional drivers. In the conventional driver shown in Figure 1(a), the positive stepped-up voltage is generated to drive the LED's anodes by using a boost converter [1-6] or a step-up SC DC-DC converter [7-25]. Thus, when the LEDs are mismatched, the converter must switch to step-up mode due to the bad forward voltage of only one LED.

To overcome this problem, the driver circuit shown in Figure 1(b) [27] has been proposed. In the conventional driver shown in Figure 1(b), the negative stepped-down voltage is generated to drive the LED's cathode only when the input voltage is insufficient to drive $1\times$ transfer mode. Therefore, the conventional driver shown in Figure 1(b) can achieve high power efficiency. However, the conventional driver shown in Figure 1(b) is difficult to improve power efficiency further, because the conversion ratio of the $-0.5\times$ charge pump is predetermined by circuit structure.

3. **Proposed WLED Driver.** Figure 2 shows the block diagram of the proposed driver. Unlike conventional drivers shown in Figure 1, the proposed driver has the dual-input structure with battery-charge process. Figure 3 shows the circuitry of the proposed driver. According to the voltage of solar-cells, the proposed converter changes the operation modes as shown in Table 1.

When voltage V_{in2} of solar-cells is sufficient to drive all LEDs, the proposed driver is operated at Mode-1. In the case of Mode-1, the LED's anodes are driven by V_{in2}, where the LED's cathodes are grounded via MUX. On the other hand, when V_{in2} is insufficient

TABLE 1. Timing of clock pulses

	Phase	On	Off	State of battery
Mode-1	——	S_2	S_1, S_3, S_4	——
Mode-2	Charging	S_1, S_2	S_3, S_4	Discharging
	Transfer	S_2	S_1, S_3, S_4	
Mode-3	Charging	S_3, S_4	S_1, S_2	Charging
	Transfer	S_4	S_1, S_2, S_3	

TABLE 2. Comparison of features

	Approach-1	Approach-2	Approach-3
Type	WLED driver using a step-up converter	Negative SC-based driver	Proposed driver
Individual mode switching	NG	OK	OK
Energy-saving using clean energy	NG	NG	OK
No flux of magnetic induction	OK : Charge pump NG : Boost converter	OK	NG
Controllability of conversion ratio	NG : Charge pump OK : Boost converter	NG	OK

to drive LEDs, the proposed driver is operated at Mode-2. In the case of Mode-2, the bi-direction buck-boost converter generates the negative stepped-down voltage to drive the LED's cathode. Unlike charge-pumps [27] and SC DC-DC converters [7-26], the proposed driver can adjust the output voltage by controlling the duty factor of clock pulses. Thus, in spite of the voltage change in solar-cells, the proposed driver can keep the output voltage constant by controlling the duty factor.

When the LED back-light is standby mode, the proposed driver is operated at Mode-3. In the case of Mode-3, the proposed driver charges a rechargeable battery. In the battery-charge process, the bi-direction buck-boost converter provides the positive stepped-up voltage to the battery. Hence, the proposed driver provides us to achieve long battery lifetime.

Table 2 shows the summary of the comparison between the proposed driver and the conventional drivers. As Table 2 shows, the weak point of the proposed driver is the flux of magnetic induction. However, the proposed driver can alleviate the energy consumption of the battery by utilizing solar energy. Furthermore, owing to the controllability of conversion ratio, the proposed driver can keep the output voltage constant in spite of the voltage reduction of solar-cells caused by shadow.

To clarify the operation of the proposed driver, the theoretical analysis concerning the output voltage will be described in the following subsections. For the sake of simplicity of circuit analyses, we assume that on-resistances R_{on1}, R_{on2}, R_{on3}, R_{on4}, R_{d1} and R_{d2} of switches S_1, S_2, S_3, S_4, D_1 and D_2 are negligibly small.

3.1. **Mode-1.** When voltage V_{in2} of solar-cells is sufficient to drive all LEDs, the proposed driver is set to Mode-1. Figure 4 shows the instantaneous equivalent circuit in the case

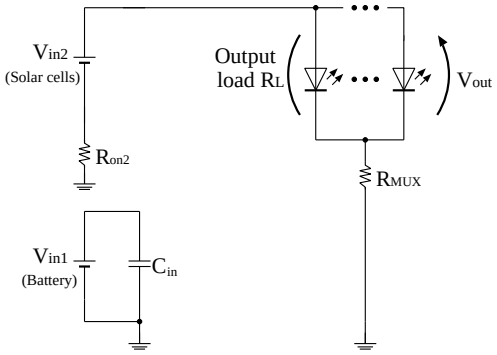

FIGURE 4. Instantaneous equivalent circuit in the case of Mode-1

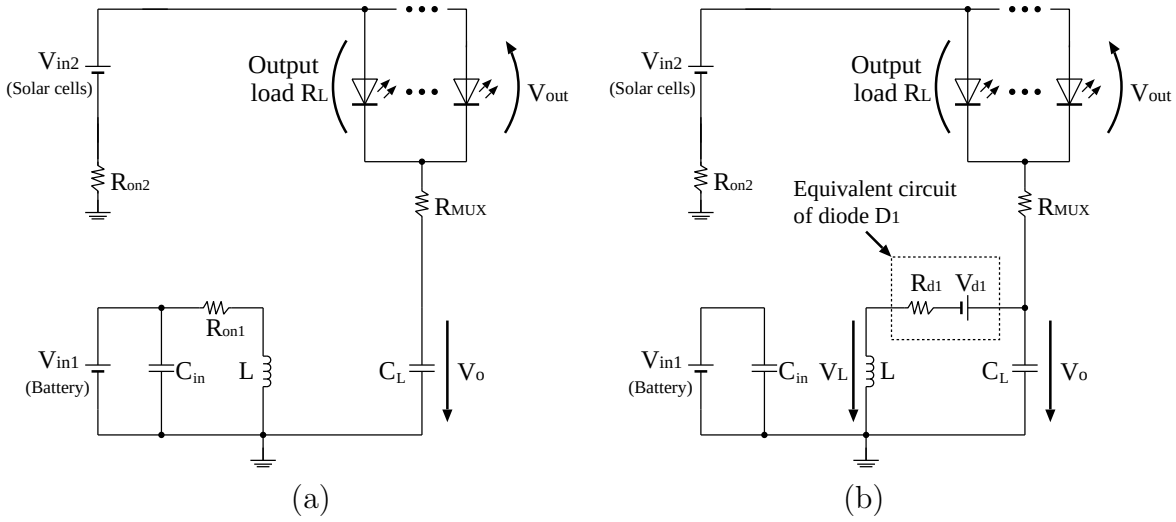

FIGURE 5. Instantaneous equivalent circuits in the case of Mode-2, (a) Charging, (b) Transfer

of Mode-1. In Figure 4, output voltage V_{out} is given by

$$\begin{aligned} V_{out} &= \frac{R_L}{R_L + R_{MUX}} \times V_{in2} \\ &\simeq V_{in2}, \end{aligned} \tag{1}$$

where $R_L \gg R_{MUX}$. In (1), R_{MUX} denotes the on-resistance of multiplexer MUX. As (1) shows, battery energy is not consumed. In this case, LEDs are driven by using solar energy provided by V_{in2}.

3.2. **Mode-2.** When voltage V_{in2} of solar-cells is insufficient to drive LEDs, the LEDs are driven by using the energy provided by V_{in1} and V_{in2}. In the case of Mode-2, the converter block shown in Figure 3 generates negative stepped-down voltage. Figure 5 shows instantaneous equivalent circuits in the case of Mode-2, where V_{d1} denotes the threshold voltage of diode D_1. During switch S_1 is in the on-state (see Figure 5(a)), the input voltage source is directly connected to inductor L. Thus, energy is stored in L whereas capacitor C_L supplies energy to output load R_L. On the other hand, during S_1 is in the off-state (see Figure 5(b)), inductor L is connected to R_L and C_L. In this timing, the energy is transferred from L to C_L and R_L.

In the case of Mode-2, the operation of the proposed driver can be divided into two modes: continuous mode and discontinuous mode. In continuous mode, output voltage

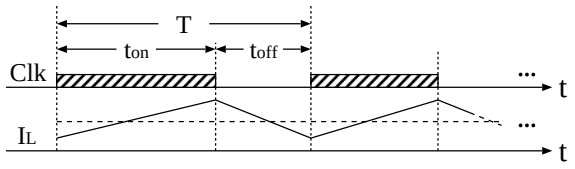

FIGURE 6. Waveform of inductor current I_L in continuous mode

V_{out} of the proposed driver can be obtained by the following method. Figure 6 shows the current of inductor L, I_L, in the continuous mode. At the end of on-state and off-state, the variation of I_L can be expressed as

$$\Delta I_{Lon} = \int_0^{DT} \frac{V_{in1}}{L} dt = \frac{V_{in1} DT}{L} \tag{2}$$

$$\text{and} \qquad \Delta I_{Loff} = \int_0^{(1-D)T} \frac{V_L}{L} dt = \frac{V_L (1-D) T}{L}, \tag{3}$$

where D is the duty factor and T is the period of clock pulses. Here, the relation between (2) and (3) is given by

$$\Delta I_{Lon} + \Delta I_{Loff} = 0, \tag{4}$$

because the variation of I_L during on-state and off-state must be zero. From (2), (3) and (4), voltage V_o is derived as follows:

$$\begin{aligned} V_o &= V_{d1} + V_L \\ &= V_{d1} - \left(\frac{D}{1-D} \right) V_{in1}. \end{aligned} \tag{5}$$

Finally, using (2), (3), (4) and (5), we have the output voltage V_{out} as follows:

$$\begin{aligned} V_{out} &= (V_{in2} - V_o) \times \frac{R_L}{R_L + R_{MUX}} \\ &= \left\{ V_{in2} - V_{d1} + \left(\frac{D}{1-D} \right) V_{in1} \right\} \times \frac{R_L}{R_L + R_{MUX}}. \end{aligned} \tag{6}$$

Especially, if $R_L \gg R_{MUX}$, (6) can be rewritten as

$$V_{out} \simeq V_{in2} - V_{d1} + \left(\frac{D}{1-D} \right) V_{in1}. \tag{7}$$

As (7) shows, the proposed driver can adjust output voltage V_{out} by controlling duty factor D. For example, output voltage V_{out} becomes 3.5 V if $V_{in1} = 3$ V, $V_{in2} = 2$ V, $V_{d1} = 0.5$ V and $D = 0.4$. In (7), output voltage V_{out} must satisfy

$$V_{out} \geq V_{LED} \ (= 3.5 \sim 3.8\,\text{V}), \tag{8}$$

where V_{LED} denotes the sufficient voltage to drive LEDs. Therefore, the condition of duty factor D is given by

$$D \geq \frac{\left(\frac{R_L + R_{MUX}}{R_L} \right) V_{LED} + V_{d1} - V_{in2}}{V_{in1} + \left(\frac{R_L + R_{MUX}}{R_L} \right) V_{LED} + V_{d1} - V_{in2}}. \tag{9}$$

Especially, if $R_L \gg R_{MUX}$, (9) can be rewritten as

$$D \geq \frac{V_{LED} + V_{d1} - V_{in2}}{V_{in1} + V_{LED} + V_{d1} - V_{in2}}. \tag{10}$$

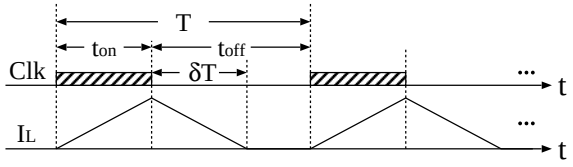

FIGURE 7. Waveform of inductor current I_L in discontinuous mode

For example, duty factor D must satisfy $D \geq 0.43$ if $V_{in1} = 3$ V, $V_{in2} = 2$ V, $V_{d1} = 0.5$ V and $V_{LED} = 3.8$ V.

On the other hand, in discontinuous mode, output voltage V_{out} can be obtained by the following method. Figure 7 shows the current of inductor L, I_L, in the discontinuous mode. The feature of discontinuous mode is that the inductor is completely discharged at the end of off-state. At the end of on-state, the variation of I_L can be expressed as

$$\Delta I_{Lon} = \int_0^{DT} \frac{V_{in1}}{L} dt = \frac{V_{in1} DT}{L}. \tag{11}$$

On the hand, at the end of off-state, the variation of I_L can be expressed as

$$\Delta I_{Loff} = \int_0^{\delta T} \frac{V_o}{L} dt = \frac{V_o \delta T}{L}, \tag{12}$$

because inductor current I_L becomes zero after δT during off-state. Here, average power P_{in1} which is supplied from V_{in1} is given by

$$P_{in1} = \frac{1}{2} V_{in1} \Delta I_{Lon} \frac{DT}{T}. \tag{13}$$

Furthermore, average power P_{in1} can be expressed also as the following:

$$P_{in1} = V_L^2 / \left\{ \frac{V_L (R_L + R_{MUX})}{V_L + (V_{in2} - V_{d1})} \right\}, \tag{14}$$

because the energy supplied from V_{in1} is consumed by R_L and R_{MUX}. Therefore, from (11), (12), (13) and (14), the following equation is obtained:

$$V_L = -\frac{(V_{in2} - V_{d1})\sqrt{Lf} + \sqrt{(V_{in2} - V_{d1})^2 Lf + 2D^2 V_{in1}^2 (R_L + R_{MUX})}}{2\sqrt{Lf}}, \tag{15}$$

where $f = 1/T$. Finally, output voltage V_{out} can be expressed as

$$\begin{aligned} V_{out} &= \{V_{in2} - (V_{d1} + V_L)\} \times \frac{R_L}{R_L + R_{MUX}} \\ &= \frac{3R_L (V_{in2} - V_{d1})}{2(R_L + R_{MUX})} + \frac{R_L \sqrt{(V_{in2} - V_{d1})^2 Lf + 2D^2 V_{in1}^2 (R_L + R_{MUX})}}{2\sqrt{Lf}(R_L + R_{MUX})}. \end{aligned} \tag{16}$$

Especially, if $R_L \gg R_{MUX}$, (16) can be rewritten as

$$V_{out} = \frac{3(V_{in2} - V_{d1})}{2} + \frac{\sqrt{(V_{in2} - V_{d1})^2 Lf + 2D^2 V_{in1}^2 R_L}}{2\sqrt{Lf}}. \tag{17}$$

The limit between continuous mode and discontinuous mode can be derived as follows. In the limit condition, inductor current I_L becomes zero at the end of on-state and off-state as shown in Figure 8. Therefore, average power P_{in1} is given by (13), where ΔI_{Lon} is given by (2). Furthermore, average power P_{in1} can be expressed also as (14), where V_L

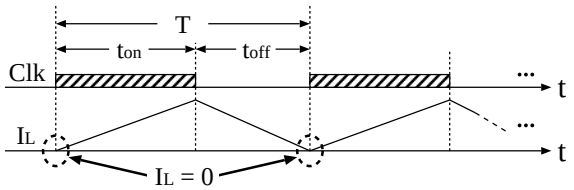

FIGURE 8. Waveform of inductor current I_L in limit condition

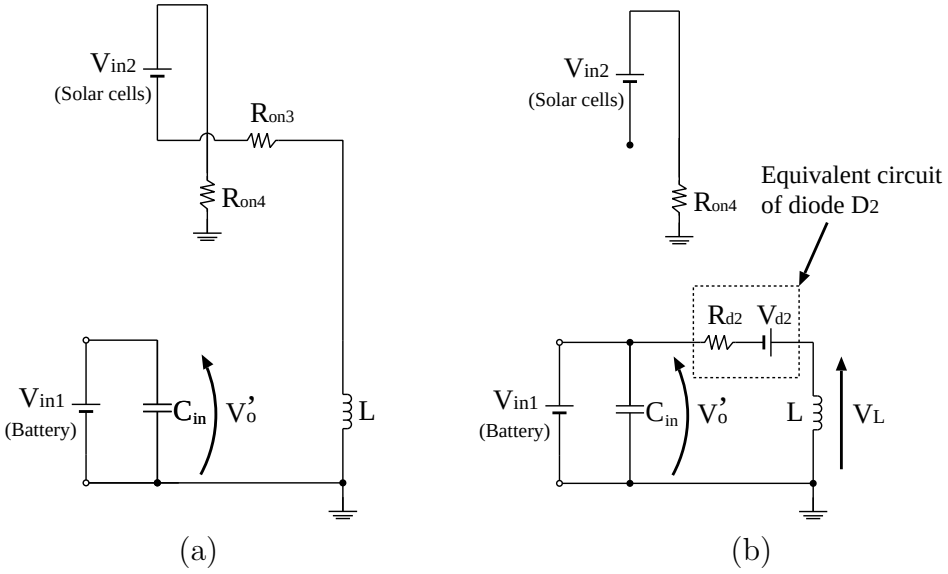

FIGURE 9. Instantaneous equivalent circuits in the case of Mode-3, (a) Charging, (b) Transfer

can be obtained by (2), (3) and (4). From (2), (3), (4) and (14), the following equation can be derived:

$$P_{in1} = \left\{ \left(\frac{D}{1-D} \right)^2 V_{in1}^2 - \left(\frac{D}{1-D} \right) (V_{in2} - V_{d1}) V_{in1} \right\} \times \frac{1}{R_L + R_{MUX}}. \tag{18}$$

Thus, from (2), (13) and (18), the limit resistance can be given by

$$R_L = \frac{2Lf\{DV_{in1} - (V_{in2} - V_{d1})(1-D)\}}{D(1-D)^2 V_{in1}} - R_{MUX}. \tag{19}$$

Especially, if $R_{MUX} \simeq 0$, (19) can be rewritten as

$$R_L = \frac{2Lf\{DV_{in1} - (V_{in2} - V_{d1})(1-D)\}}{D(1-D)^2 V_{in1}}. \tag{20}$$

For example, output load R_L becomes $R_L \simeq 472\ \Omega$ if $V_{in1} = 3$ V, $V_{in2} = 2$ V, $V_{d1} = 0.5$ V, $D = 0.4$, $L = 0.68$ mH and $f = 500$ kHz.

3.3. **Mode-3.** When the LEDs are off, the rechargeable battery connected to terminal V_{in1} is charged by using solar energy. In the case of Mode-3, the converter block shown in Figure 3 provides positive stepped-up voltage to the battery. Figure 9 shows the instantaneous equivalent circuits in the case of Mode-3, where V_{d2} denotes the threshold voltage of diode V_{d2}. In Figure 9, voltage $V_o^{'}$ which is provided to the battery can be obtained by the following method.

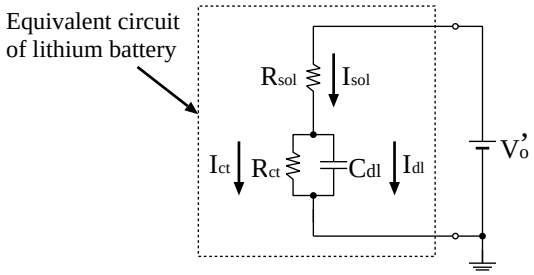

FIGURE 10. Equivalent circuit of a lithium battery

At the end of on-state and off-state, the variation of I_L can be expressed as

$$\Delta I_{Lon} = -\int_0^{DT} \frac{V_{in2}}{L} dt = -\frac{V_{in2} DT}{L} \tag{21}$$

$$\text{and} \qquad \Delta I_{Loff} = \int_0^{(1-D)T} \frac{V_L}{L} dt = \frac{V_L (1-D) T}{L}. \tag{22}$$

Here, the relation between (21) and (22) is given by (4), because the internal resistance of the lithium battery is small. Finally, using (4), (21) and (22), output voltage $V_o^{'}$ can be obtained by

$$\begin{aligned} V_o^{'} &= V_L - V_{d2} \\ &= \left(\frac{D}{1-D} \right) V_{in2} - V_{d2}. \end{aligned} \tag{23}$$

For example, voltage $V_o^{'}$ becomes $V_o^{'} \simeq 3.2$ V if $V_{in2} = 2$ V, $V_{d2} = 0.5$ V and $D = 0.65$. In (23), output voltage $V_o^{'}$ must satisfy

$$V_o^{'} \geq V_{in1}. \tag{24}$$

Therefore, the condition of duty factor D is given by

$$D \geq \frac{V_{in1} + V_{d2}}{V_{in1} + V_{in2} + V_{d2}}. \tag{25}$$

For example, duty factor D must satisfy $D \geq 0.64$ if $V_{in1} = 3$ V, $V_{in2} = 2$ V and $V_{d2} = 0.5$ V.

When the internal resistance of the lithium battery is small, the battery is charged by using voltage $V_o^{'}$ shown in (23). Thus, the battery-charge process can be modeled by the equivalent circuit shown in Figure 10, where R_{sol}, R_{ct} and C_{dl} denote the solution resistance, the charge transfer resistance and the double layer capacitance, respectively. In Figure 10, the following equations are derived by using the Kirchhoff's law:

$$I_{sol} = I_{ct} + I_{dl}, \tag{26}$$

$$R_{ct} I_{ct} = \frac{q_{dl}}{C_{dl}} \tag{27}$$

$$\text{and} \qquad V_o^{'} = R_{sol} \frac{dq_{sol}}{dt} + \frac{q_{dl}}{C_{dl}}, \tag{28}$$

where q_{sol}, q_{ct} and q_{dl} denote electric charges of I_{sol}, I_{ct} and I_{dl}, respectively. From (26), (27) and (28), the following ordinary-differential-equation is obtained:

$$V_o^{'} = R_{sol} \frac{dq_{dl}}{dt} + \left(\frac{R_{ct} + R_{sol}}{R_{ct} C_{dl}} \right) q_{dl}. \tag{29}$$

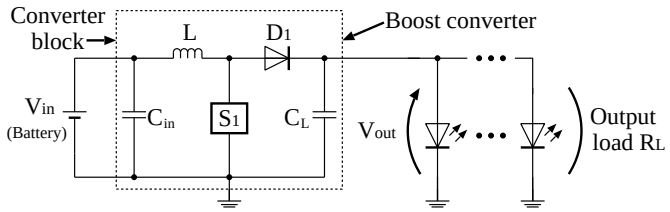

FIGURE 11. Conventional inductor-based driver using a boost converter

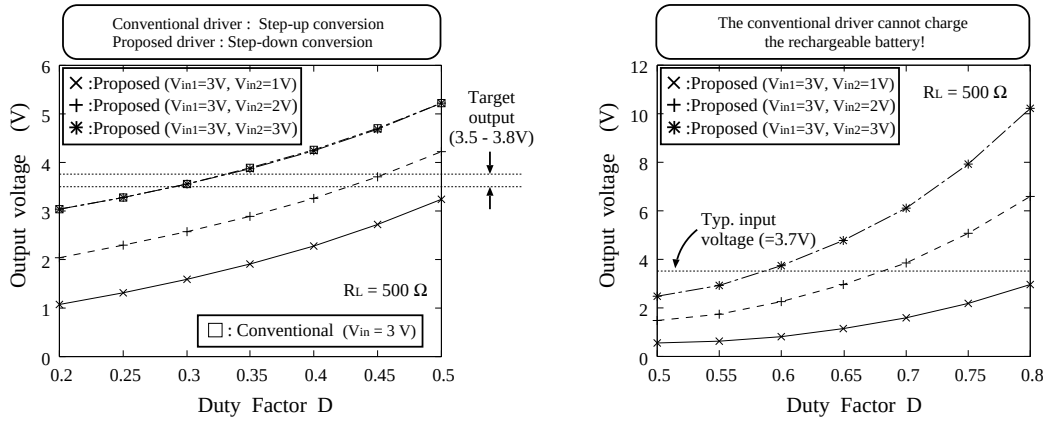

FIGURE 12. Simulated output voltage as a function of duty factor, (a) LED drive (Mode-2), (b) Batter charge (Mode-3)

Solving (29), the voltage of capacitor C_{dl}, V_{Cdl}, can be expressed as

$$\begin{aligned} V_{Cdl} &= V_o^{'}\left(\frac{R_{ct}}{R_{ct}+R_{sol}}\right)\left[1-\exp\left\{-\left(\frac{R_{ct}+R_{sol}}{R_{sol}R_{ct}C_{dl}}\right)t\right\}\right] \\ &\quad +V_{ini}\exp\left\{-\left(\frac{R_{ct}+R_{sol}}{R_{sol}R_{ct}C_{dl}}\right)t\right\}, \end{aligned} \tag{30}$$

where V_{ini} denotes the initial voltage of C_{dl}. Especially, if the initial electric charge of C_{dl} is zero, (30) can be rewritten as

$$V_{Cdl} = V_o^{'}\left(\frac{R_{ct}}{R_{ct}+R_{sol}}\right)\left[1-\exp\left\{-\left(\frac{R_{ct}+R_{sol}}{R_{sol}R_{ct}C_{dl}}\right)t\right\}\right]. \tag{31}$$

As (30) and (31) show, the voltage of the lithium battery rises exponentially.

4. **Simulation.** To investigate characteristics of the proposed driver, SPICE simulations were performed concerning the proposed driver shown in Figure 3 and the conventional driver shown in Figure 11. The conventional driver shown in Figure 11 is the inductor-based WLED driver using a boost converter.

Figures 12 and 13 [1] show the simulated output voltage and the simulated power efficiency [2] , respectively. In the SPICE simulations of Figures 12 and 13, the power switch and the diode were modeled by using SPICE macro-model, where $C_{in} = C_L = 5$ μF, $L = 0.68$ mH, $R_L = 500$ Ω, $R_{on} = R_{MUX} = 1$ Ω and $T = 2$ μs. In Figure 12(a), the

[1]In Figure 13, power efficiency η was calculated by $\eta = P_{out}/(P_{in1} + P_{in2})$, where P_{out} is the output power, P_{in1} and P_{in2} are the input power for input V_{in1} and V_{in2}, respectively.

[2]To save space, only the characteristics in Mode-2 and Mode-3 are shown in this manuscript, because the circuit characteristics in Mode-1 are obvious.

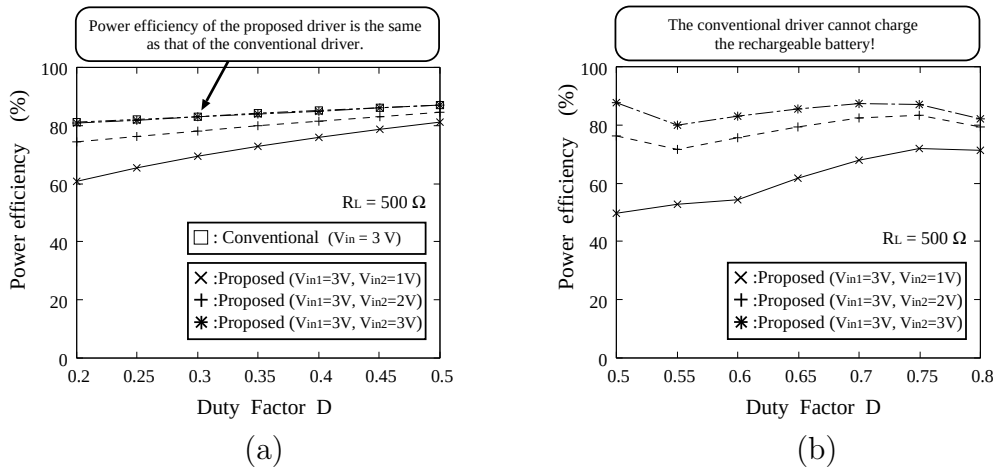

FIGURE 13. Simulated power efficiency as a function of duty factor, (a) LED drive (Mode-2), (b) Batter charge (Mode-3)

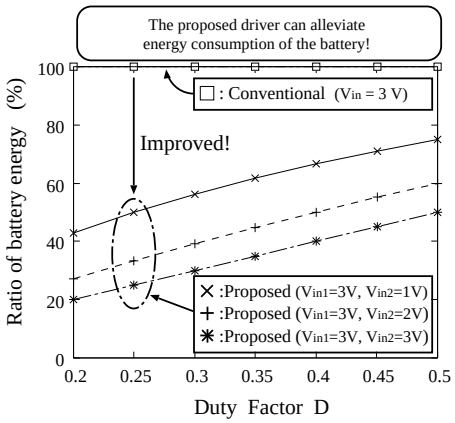

FIGURE 14. Ratio of battery energy obtained by SPICE simulations

output voltage of the conventional driver is provided by stepping up V_{in}. On the other hand, the output voltage of the proposed driver is provided by compensating solar input V_{in2} with battery input V_{in1}. As Figure 12(a) shows, in spite of variation in V_{in2}, the proposed driver can generate sufficient voltage to drive LEDs by using solar energy and battery energy. Furthermore, the tendency of output characteristics in Figures 12(a) and (b) corresponds well with (6) and (23), respectively.

In SPICE simulations of Figures 12(b) and 13(b), the battery was modeled by using the equivalent circuit shown in Figure 10, where R_{sol}, R_{ct} and C_{dl} were set to $R_{sol} = 5\ \Omega$, $R_{ct} = 1\ \text{k}\Omega$ and $C_{dl} = 50\ \mu\text{F}$, respectively. As Figure 12(b) shows, the proposed driver provides the stepped-up solar voltage to charge the rechargeable battery, because the proposed driver can achieve the bi-directional conversion. On the other hand, the conventional driver cannot charge the rechargeable battery, because the conventional driver performs the unidirectional conversion.

Figure 14 shows the ratio of battery energy used to drive LEDs. As Figure 14 shows, the ratio of battery energy in the proposed driver is much smaller than that of the conventional driver, because LEDs are driven by using not only battery energy but also solar energy. Therefore, the proposed driver can alleviate the energy consumption of the battery.

The result of the comparison between the proposed driver and the conventional driver is as follows: As Figure 13(a) shows, the power efficiency of the conventional converter is

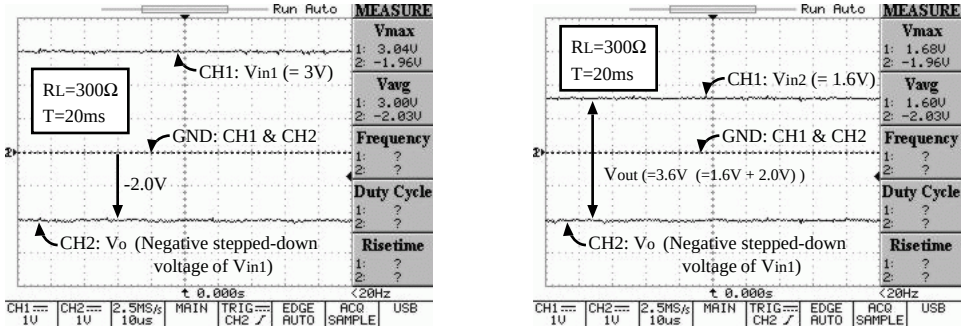

(a) (b)

FIGURE 15. Measured output voltage of the experimental circuit in the case of Mode-2, (a) V_{in1} and V_o, (b) V_{in2} and V_o

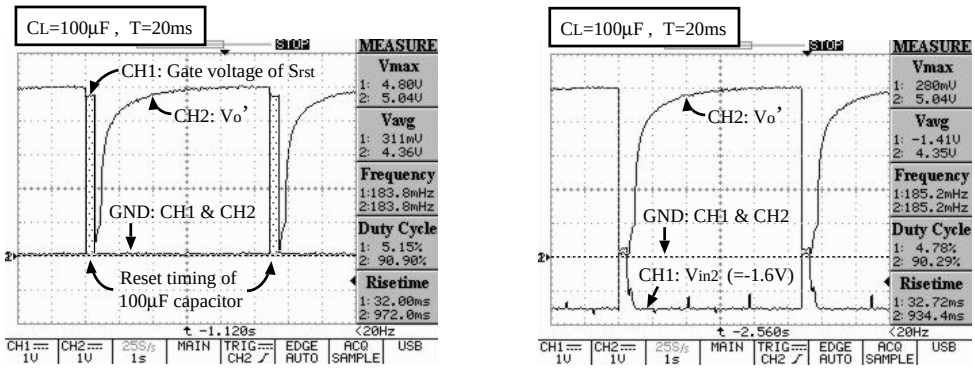

(a) (b)

FIGURE 16. Measured output voltage of the experimental circuit in the case of Mode-3, (a) $V_o^{'}$ and gate voltage of S_{rst}, (b) $V_o^{'}$ and V_{in2}

almost the same as that of the proposed driver when the input voltages V_{in1} and V_{in2} are 3 V. However, as Figures 12(b) and 14 show, the proposed driver can achieve long battery lifetime.

5. **Experiment.** To confirm the validity of circuit design, experiments were performed. Figure 15 shows the measured output voltage in the case of Mode-2. The experimental circuit was built with commercially available parts: power transistor 2SK2493 and Schottky barrier diode 11EQS03. In Figure 15, the experiments were performed under conditions where $V_{in1} = 3$ V, $V_{in2} = 1.6$ V, $C_{in} = C_L = 10$ μF, $L = 4.7$ mH, $R_L = 300$ Ω and $T = 20$ ms. As Figure 15 shows, the experimental circuit can offer the sufficient output voltage by compensating V_{in2} with stepped-down V_{in1}. From Figure 15, the validity of the circuit design can be confirmed [3].

Figure 16 shows the charge process obtained by experiments, where capacitor $C_{bat} = 100$ μF was connected to terminal-V_{in1} in substitution for the lithium battery [4] to reduce the experiment time. In the experimental circuit, in order to confirm the charge process, reset

[3]In the experiment, circuit properties such as power efficiency, ripple noise, etc. were not examined, because the experimental circuit was built with commercially available transistors on the bread board. For example, unlike an IC chip, the parasitic resistance of the experimental circuit synthesized with discrete elements is very large. Therefore, only the circuit design was verified in this experiment.

[4]To charge lithium batteries, a charge controller which provides a constant voltage or constant current configuration is necessary. The development of the charge controller is left to a future study.

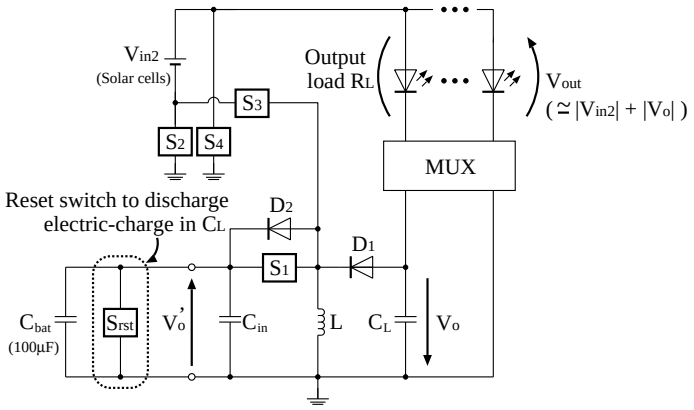

FIGURE 17. Experimental circuit to investigate charge process

switch S_{rst} was attached to terminal-V_{in1} as shown in Figure 17. As Figure 16 shows, the proposed driver circuit can charge the battery by converting V_{in2}, where solar input V_{in2} was set to 1.6 V [5]. Therefore, long battery lifetime will be realized by the proposed driver. Furthermore, as shown in (31), measured voltage $V_o^{'}$ in Figure 16 rises exponentially.

6. **Conclusions.** Aimed at back-lighting applications, a dual-input WLED driver using a bi-direction buck-boost converter has been proposed in this paper. Through SPICE simulations and experiments, the characteristics of the proposed driver were investigated. SPICE simulations showed that the proposed driver can generate sufficient voltage to drive LEDs by using solar energy and battery energy. Unlike conventional drivers using a positive step-up converter, the individual mode switching enables the proposed driver to improve power efficiency. Furthermore, SPICE simulations showed that the proposed converter can adjust the output voltage by controlling the duty factor. Therefore, when output voltage V_{out} is $V_{out} \gg 3.5 \sim 3.8$ V, the proposed driver can achieve higher power efficiency than the conventional negative charge pump. Next, the validity of circuit design was confirmed by experiments. By employing a bi-direction buck-boost converter, the proposed driver circuit can achieve long battery lifetime, because the battery-charge process was confirmed through experiments. The development of the peripheral circuit to control the battery charge effectively is left to a future study.

REFERENCES

[1] S. Banerjee, A. L. Baranovski, J. L. R. Marrero and O. Woywode, Minimizing electromagnetic interference problems with chaos, *IEICE Fundamentals*, vol.E87-A, no.8, pp.2100-2109, 2004.

[2] T. Kabe, S. Parui, H. Torikai, S. Banerjee and T. Saito, Analysis of piecewise constant models of current mode controlled DC-DC converters, *IEICE Fundamentals*, vol.E90-A, no.2, pp.448-456, 2007.

[3] R. Y. Kim, J. S. Lai, B. York and A. Koran, Analysis and design of maximum power point tracking scheme for thermoelectric battery energy storage system, *IEEE Trans. Industrial Electronics*, vol.56, no.9, pp.3709-3716, 2009.

[4] D. K. Kwak, A new boost dc-dc converter of high efficiency by using a partial resonant circuit, *IEICE Electronics EXpress*, vol.6, no.12, pp.844-850, 2009.

[5] S. Fan, K. Wang and L. Geng, Design and implementation of a mixed-signal boost converter with a novel multi-phase clock DPWM, *IEICE Electronics EXpress*, vol.7, no.14, pp.1091-1097, 2010.

[6] T. Yasufuku, K. Ishida, S. Miyamoto, H. Nakai, M. Takamiya, T. Sakurai and K. Takeuchi, Inductor and TSV design of 20-V boost converter for low power 3D solid state drive with NAND flash memories, *IEICE Electronics*, vol.E93-C, no.3, pp.317-323, 2010.

[5] As Figures 9 and 16(b) show, the inverted V_{in2} is provided to the converter block.

[7] T. Tanzawa and T. Tanaka, A dynamic analysis of the Dickson charge pump circuit, *IEEE, J. Solid-State Circuits*, vol.32, no.8, pp.1237-1240, 1997.
[8] T. Myono, A. Uemoto, S. Kawai, E. Nishibe, S. Kikuchi, T. Iijima and H. Kobayashi, High-efficiency charge-pump circuits with large current output for mobile equipment applications, *IEICE, Electronics*, vol.E84-C, no.10, pp.1602-1611, 2001.
[9] J. A. Starzyk, T. W. Jan and F. Qiu, A DC-DC charge pump design based on voltage doublers, *IEEE Trans. Circuit & Syst.-I*, vol.48, no.3, pp.350-359, 2001.
[10] K. Min and J. Ahn, CMOS charge pumps using cross-coupled charge transfer switches with improved voltage pumping gain and low gate-oxide stress for low-voltage memory circuits, *IEICE, Electronics*, vol.E85-C, no.1, pp.225-229, 2002.
[11] K. Yamada, N. Fujii and S. Takagi, Capacitance value free switched capacitor DC-DC voltage converter realizing arbitrary rational conversion ratio, *IEICE, Fundamentals*, vol.E87-A, no.2, pp.344-349, 2004.
[12] B. R. Gregoire, A compact switched-capacitor regulated charge pump power supply, *IEEE J. Solid-State Circuits*, vol.41, no.8, pp.1944-1953, 2006.
[13] C. L. Wei, L. Y. Wu, H. H. Yang, C. H. Tsai, B. D. Liu and S. J. Chang, A versatile step-up/step-down switched-capacitor-based DC-DC converter, *IEICE, Electronics*, vol.E91-C, no.5, pp.809-812, 2008.
[14] T. Yamakawa, T. Inoue and A. Tsuneda, Design and experiments of a novel low-ripple Cockcroft-Walton AC-to-DC converter for a coil-coupled passive RFID tag, *IEICE, Fundamentals*, vol.E91-A, no.2, pp.513-520, 2008.
[15] J. H. Bong, Y. J. Kwon, D. Kim and K. S. Min, Negative charge pump circuit with large output current and high power efficiency, *IEICE Electronics EXpress*, vol.6, no.6, pp.304-309, 2009.
[16] K. Eguchi, I. Oota, S. Terada and T. Inoue, A design method of switched-capacitor power converters by employing a ring-type power converter, *International Journal of Innovative Computing, Information and Control*, vol.5, no.10(A), pp.2927-2938, 2009.
[17] I. Doms, P. Merken, C. V. Hoof and R. P. Mertens, Capacitive power management circuit for micropower thermoelectric generators with a 1.4μA controller, *IEEE, J. Solid-State Circuits*, vol.44, no.10, pp.2824-2833, 2009.
[18] S. J. Park, Y. G. Kang, J. Y. Kim, T. H. Han, Y. H. Jun, C. Lee and B. S. Kong, CMOS cross-coupled charge pump with improved latch-up immunity, *IEICE Electronics EXpress*, vol.6, no.11, pp.736-742, 2009.
[19] I. Y. Chung and J. Shin, New charge pump circuits for high output voltage and large current drivability, *IEICE Electronics EXpress*, vol.6, no.12, pp.800-805, 2009.
[20] K. Eguchi, S. Pongswatd, K. Tirasesth, H. Sasaki and T. Inoue, Optimal design of a single-input parallel DC-DC converter designed by switched capacitor techniques, *International Journal of Innovative Computing, Information and Control*, vol.6, no.1, pp.215-227, 2010.
[21] S. Byun and J. H. Shim, Charge pump circuit with wide range digital leakage current mismatch compensator, *IEICE Electronics EXpress*, vol.7, no.23, pp.1709-1713, 2010.
[22] K. Eguchi, I. Oota, S. Pongswatd, A. Julsereewong, K. Tirasesth and H. Sasaki, Synthesis and analysis of a dual-input parallel DC-DC converter designed by using switched capacitor techniques, *International Journal of Innovative Computing, Information and Control*, vol.7, no.4, pp.1675-1688, 2011.
[23] P. H. Chen, K. Ishida, X. Zhang, Y. Okuma, Y. Ryu, M. Takamiya and T. Sakurai, 0.18-V input charge pump with forward body bias to startup boost converter for energy harvesting applications, *IEICE, Electronics*, vol.E94-C, no.4, pp.598-604, 2011.
[24] W. Oh and P. Nadimpalli, A low noise regulated charge pump circuit, *IEICE Electronics EXpress*, vol.8, no.7, pp.416-422, 2011.
[25] K. Eguchi, S. Pongswatd, K. Tirasesth, I. Oota, H. Sasaki and T. Inoue, A switched-capacitor-based serial DC-DC converter using clean energy power supplies, *International Journal of Innovative Computing, Information and Control*, vol.7, no.6, pp.3485-3498, 2011.
[26] K. Eguchi, S. Pongswatd, K. Tirasesth, K. Fujimoto, H. Sasaki and T. Inoue, A step-down switched-capacitor AC-DC converter for energy harvesting system using vibration-based energy, *International Journal of Innovative Computing, Information and Control*, vol.7, no.7(A), pp.3739-3750, 2011.
[27] J. Kim, Negative charge pumps achieve inductor-like efficiency for WLED backlights, *MAXIM Engineering Journal*, vol.64, pp.13-15, 2008.